Physicochem. Probl. Miner. Process., 59(4), 2023, 172683

http://www.journalssystem.com/ppmp

Physicochemical Problems of Mineral Processing

ISSN 1643-1049

Crystal-to-crystal investigations of highly thermally stable three-dimensional coordination polymer based on sodium(I) ions and 4,4′-stilbenedicarboxylic acid

Marcin Groszek, Renata Łyszczek, Agnieszka Ostasz and Dmytro Vlasyuk

Department of General and Coordination Chemistry and Crystallography, Faculty of Chemistry, Institute of Chemical Sciences, Maria Curie-Sklodowska University, Maria Curie-Sklodowska Sq. 2, 20-031 Lublin, Poland

Corresponding author: marcin.groszek@mail.umcs.pl (Marcin Groszek)

Abstract: The new three-dimensional coordination polymer termed $\{[Na_2SDC(H_2O)]\}_n$ (SDC^{2-}= $C_{16}H_{10}O_4^{2-}$) has been synthesized using workstation Easymax 102 while controlling the conditions and monitoring *in-situ* reagents. The metal complex was obtained in the reaction of sodium hydroxide with a suspension of 4,4′-stilbenedicarboxylic acid in aqueous medium. The compound was characterized by elemental analysis, single crystal, and powder X-ray diffraction methods, ATR-FTIR spectroscopy, SEM and optical microscopy, TG-DSC and TG-FTIR thermal analysis in air and nitrogen atmosphere. In the crystal structure of $\{[Na_2SDC(H_2O)]\}_n$ appears penta- and hexacoordinated sodium atoms joined by octa- and decadentate SDC^{2-} linkers. Aqua ligand acts as bridge between Na1 and Na2 atoms. The as-synthesized sodium complex is thermally stable up to 86°C whereas its dehydrated form has extreme stability up to 491°C. Removal of water molecule leads to the *crystal-to-crystal* transformation yielded changes in coordination modes of COO groups. Reversibility of the hydration process in the studied complex was also examined.

Keywords: coordination polymers, 4,4′stilbenedicarboxylic acid, crystal structure, thermal analysis, crystal-to-crystal transformation

1. Introduction

Coordination polymers (CPs) have become an appealing group of metal complexes since their functional properties were discovered in the 1990s (Biradha et al., 2009). The growing number of papers related to such group of compounds is related to tunable dimensionality and geometry, which with crystal nature can provide materials with a potential large surface area and adjustable pore size (Dimas et al., 2022; Wu et al. 2020; Yan et al., 2021). In addition, the synthesis of CPs is an easily scalable process, and the characterization of the obtained crystal compounds is simple using X-ray diffraction methods (Lee et al., 2021; Teo et al., 2021). Such properties of these compounds make them a very attractive materials of potential applications in various fields, including storage and separation (Fan et al., 2021; Li et al. 2022), drug delivery (Mallakpour et al., 2022; Cao et al., 2020), catalysis (Chen et al., 2021; Yang et al., 2021), proton conduction (Luo et al., 2019), and optical materials (Fu et al., 2020). Porous coordination polymers are also investigated as an ion exchangers and lightning harvesting materials (Hu et al., 2021; Fan et al., 2022).

Coordination polymers based on stilbene derivatives as organic linkers have drawn extensive attention to due to their availability, a certain degree of flexibility and luminescence properties arising from ligands (Bauer et al., 2007; Lee et al., 2013). Bridging stilbene derivatives as a rather long ligands may enhance the formation of porous structures with a very large specific surface area in which a network of channels can be distinguished. These coordination polymers show a strong affinity for gases, including the absorption of hydrogen (Wei et al., 2013) or/and the adsorption of harmful substances such as dyes (Mogale et al., 2022) and heavy metals (Omwoma et al., 2020). Another important feature in terms of stilbene-based coordination polymers application is their great thermal stability (Boxi et al.,

DOI: 10.37190/ppmp/172683

2019; Hou et al., 2020; Pe et al., 2023; Vek et al., 2022; Yu et al., 2021). This group of polymeric metal complexes shows the ligand centred emission, which is also an important property that plays the key role in their application (Kuznetsova et al., 2020). The 4,4′-stilbenedicarboxylate linker belongs to the most explored stilbene derivatives commonly used as a bridging ligand in construction of coordination polymers with different dimensionality. The vast majority of reported so far metal 4,4′-stilbenedicarboxylates contain in their structures also N-donor ligands (Allen, 2002). These ligands act as templating agent as well as introduce or strengthen some functionalities. On over 200 known crystal structures of metal complexes containing 4,4′-stilbenedicarboxylate ligand, only a few of them contain only this organic linker (Zhang et al., 2017; Ning et al., 2019; Liu et al., 2013; Deng et al., 2014; Huang et al., 2018; Li et al., 2011). Most of them were constructed from transition metal ions and lanthanides as nodes. The only reported coordination polymer from the group of alkali metals is a complex based on potassium ions (Kole et al., 2014).

To continue our research on coordination polymers based on aromatic polycarboxylate ligands (Głuchowska et al., 2022; Głuchowska et al., 2021; Łyszczek et al., 2021; Łyszczek et al., 2019; Łyszczek et al., 2022), we present the synthesis, structure, and characterization of the first sodium three-dimensional coordination polymer based on the 4,4′-stilbenedicarboxylic acid (H_2SDC). This complex was obtained from an aqueous solution utilizing EasyMax102 synthesis workstation. The morphology of formed crystals was observed by using SEM and optical microscopy. We focus on its crystal structure and coordination modes of 4,4′-stilbenedicarboxylate ligand. The influence of the aqua ligand removal of the crystal structure of sodium complex was studied. Moreover, reversibility of hydration process which leads to the *crystal-to-crystal* transformation was deeply investigated by means of ATR-FTIR spectroscopy, X-ray diffraction measurements and thermal analysis methods TG-DSC in the air and TG-FTIR coupled technique in nitrogen. The thermal stability and pathway of the decomposition of as-synthesised, dehydrated, and rehydrated forms of pristine sodium 4,4′-stilbenedicarboxylate were also explored.

2. Materials and methods

2.1. Synthesis of coordination polymer

The 4,4′-stilbenedicarboxylic acid (H_2SDC) with a purity of 95% was purchased from Angene Chemical and purified before further use. The NaOH of analytical grade was purchased from POCH S.A.

A suspension of 4,4'-stilbenedicarboxylic acid (1 mmol, 0.268 g) in 40 mL of water and a 0.1 mol/L solution of NaOH were prepared. The H_2SDC acid suspension was placed in the reaction vessel (100 mL) of the EasyMax102 (Mettler Toledo) synthesis workstation, whereas the NaOH solution was transferred to beaker from which the dosing syringe (25 mL) drew the solution added during the reaction. A multi-step procedure for compound synthesis was created in iControl 6.0 software for EasyMax102 synthesis workstation. The first step was to heat the H_2SDC acid suspension to 90°C during 10 min. and isothermally heating for 40 min. with continuous stirring. Afterwards, the NaOH solution (22 mL) was dosed into the reaction vessel with the rate of 1 mL/min. Thus, the obtained reaction mixture was heated and stirred at 90°C for further 30 minutes. Subsequently, the solution was gradually cooled (during 30 min) to 5°C and held for the next 15 minutes at such a temperature. The prepared solution slowly crystallized at room temperature until after a few days the used solvent evaporated completely and then the crystalline form of the compound was obtained. The elemental analysis for as-synthesized monocrystals $\{[Na_2SDC(H_2O)]\}_n$: Exp.: 57.39%; 3.95% for C and H, respectively, while the theoretical values are equal to: 59.14% and 3.63%.

Due to investigations of reversibility of the dehydration process in $\{[Na_2SDC(H_2O)]\}_n$, 100 mg sample of sodium complex was heated in vacuum laboratory drying oven (Salvislab) at 150°C during 2h at 0.05 mbar pressure. The obtained white polycrystalline powder was further investigated by the methods given below. In order to study the rehydration process, the 100 mg sample of dehydrated complex was stored in distilled water at room temperature for 72h. Then the sample was filtered off and dried at room temperature.

2.2. Methods

The ATR-FTIR spectra of the ligand and the obtained sodium compounds were registered in the range 4000–600 cm^{-1} by using a Nicolet 6700 (Thermo Scientific) spectrophotometer equipped with a universal ATR Smart iTR diamond attachment.

The carbon and hydrogen content were determined by elemental analysis using the CHN 2400 analyzer (Perkin-Elmer).

Thermal analyses (thermogravimetric-TG and differential scanning calorimetry-DSC) were carried out in a flowing air atmosphere (12.5 mL min^{-1}) using the SETSYS 16/18 analyser (Setaram). The samples 6-8 mg were heated in the range of 30-700°C in a ceramic crucible at a heating rate of 10°C min^{-1}. The TG–FTIR survey was performed on the Q5000 (TA) apparatus coupled with the Nicolet 6700 spectrophotometer (Thermo Scientific). The samples were heated from room temperature to 700°C with heating rate of 20°C min^{-1} in a flowing nitrogen atmosphere (25 mL min^{-1}) in platinum crucible.

The X-ray powder diffraction patterns of the studied compounds were recorded on an Empyrean diffractometer (Panalytical) over the range of 2θ=5–40° with Bragg–Brentano method (Cu-Kα radiation).

The surface area, total pore volume, average pore diameter were determined by nitrogen adsorption-desorption measured at -196°C using an automatic volumetric adsorption ASAP 2420 apparatus (Micromeritics). Incremental pore size distributions were determined from density functional theory (DFT) methods for slit pores.

Optical microscope images were taken with a polarizing filter using a Nikon Eclipse MA200, while SEM images were recorded using a Quanta 3D FEG high-resolution scanning electron-ion microscope by FEI.

Single-crystal diffraction data were collected on the Rigaku XtaLAB MM7HFMR diffractometer equipped with the "quarter-chi single" goniometer, the rotating anode generator (graphite monochromated Cu Kα radiation), and the Pilatus 200K detector. The CrysAlisPro 1.171.39.27b program was used for data collection, cell refinement, and data reduction (CrysAlisPRO Software System, 2016). The structure was solved using the direct methods implemented in the SHELXS-97 and refined with the SHELXL-18/3 program, both operating under WinGX (Farrugia, 1999; Sheldrick, 2015) [54,55].

Crystal data for $C_{16}H_{12}O_5Na_2$ (M = 330.24 g/mol): monoclinic, space group $P2_1/c$, a = 32.0997(4) Å, b = 5.80000(10) Å, c = 7.58340(10) Å, β = 91.0320(10)°, V = 1411.64(4) $Å^3$, Z = 4, Dcalc = 1.554 g/cm^3, 14074 reflections measured, 2553 unique [R_{int} = 0.0153, R_{sigma} = 0.0107] which were used in all calculations. The final R1 was 0.0277 (I > 2σ(I)) and wR2 was 0.0736 (all data). The CIF file for sodium complex was deposited at the Cambridge Crystallographic Data Centre (CCDC 2267734).

3. Results and discussion

3.1. The morphology of $\{[Na_2SDC(H_2O)]\}_n$

The three-dimensional coordination polymer of sodium(I) ions with 4,4′-stilbenedicarboxylic acid of the general formula $\{[Na_2SDC(H_2O)]\}_n$ (where $SDC^{2-}=C_{16}H_{10}O_4^{2-}$) was obtained in the reaction of sodium hydroxide with acid in aqueous solution on the EasyMax102 synthesis workstation. The scanning electron microscope (SEM) and optical microscope images were performed to investigate the morphology and microstructure of the obtained crystals. As can be seen from Fig. 1, highly soluble in water sodium 4,4′-stilbenedicarboxylate was crystallized in the form of well formulated plate rhomboidal crystals of different dimensions.

The nitrogen adsorption and desorption isotherms at -196°C were measured for pristine sample outgassed at 150°C due to investigation of its surface area. The Brauner-Emmet-Teller (BET) surface area of sample calculated from the obtained gas adsorption data is 12 m^2/g. The recorded isotherms given in Fig. 2a are of type IV according to the IUPAC classification (ALOthman, 2012). The pore size distributions for the studied complex was calculated from density functional theory. As can be seen in Fig. 2b, the pores in the complex are comprised in the range of 2-150 nm excluding microporous that classifies this material as meso- and macroporous (Xuan et al., 2012).

3.2. The crystal structure description

Single crystal X-ray analysis reveals that $\{[Na_2SDC(H_2O)]\}_n$ crystallizes in the monoclinic $P2_1/c$ space

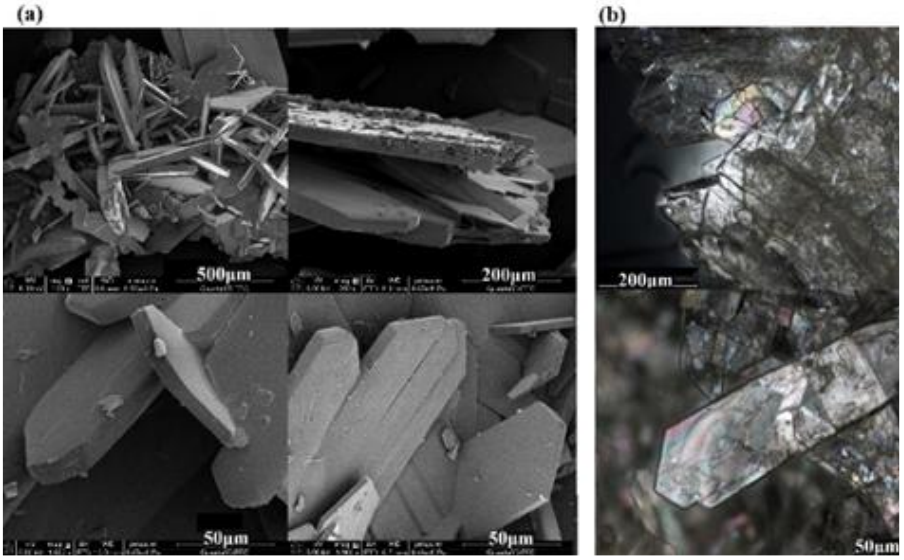

Fig 1. The images of $\{[Na_2SDC(H_2O)]\}_n$ crystals from: (**a**) SEM; (**b**) optical microscope

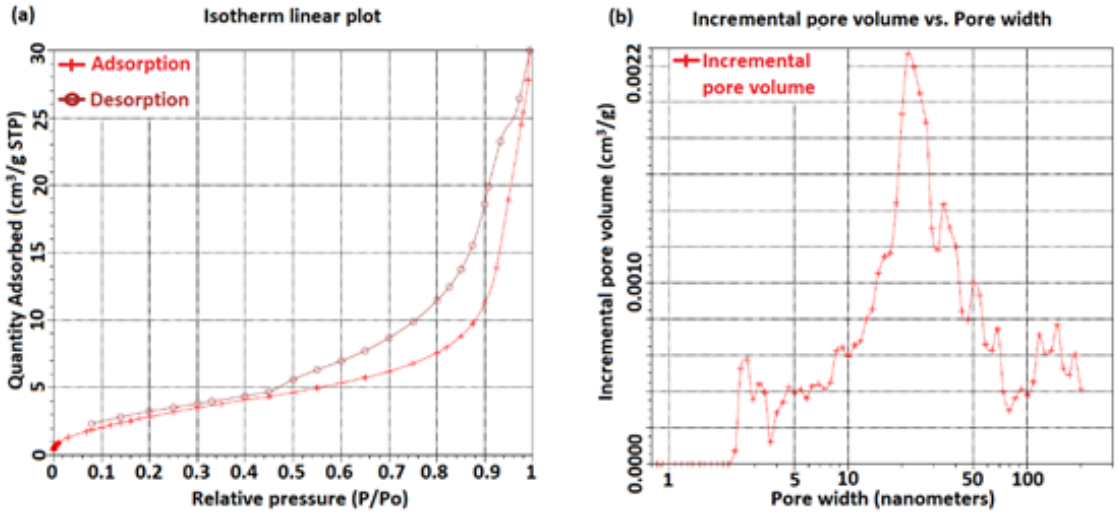

Fig 2. (a) The adsorption/desorption isotherms; (b) the DFT pore size distributions of pristine $\{[Na_2SDC(H_2O)]\}_n$

group. The asymmetric unit contains two independent sodium ions, two halves of 4,4'-stilbenedicarboxylate linker (A-SDC, B-SDC) from two independent molecules, and one water molecule (Fig. 3a). Penta-coordinated sodium Na1 atom is coordinated by four carboxylate oxygen atoms from one A-SDC and three B-SDC linkers, and one aqua ligand forming a distorted trigonal bipyramid (Fig. 3b). The coordination environment of the sodium Na2 atom consists of one aqua ligand and five carboxylate oxygen atoms from three A-SDC and one B-SDC ligands (Fig. 3a) assuming the form of a very significant distorted octahedron (Fig. 3c). The Na1-O2 bond length is 2.483(1) Å whereas Na1-O1W is slightly shorter 2.368(1) Å. The two-remaining sodium-carboxylate oxygen bonds with O2B atoms are 2.449(1) Å and 2.320(1) Å, while the Na1-O1B bond is 2.298(1) Å. Due to a significant distortion of the trigonal bipyramid, the O-Na1-O angles that would be 90° in regular polyhedron range from 77.82(4)° to 102.68(4)° while the angles that would 120° are in the 92.08(4)-134.34(4)° range. For the atom Na2 arrangement, the length bonds to $O2^a$, $O2^c$ and O1 atoms are: 2.428(1), 2.487(1) and 2.346(1) Å, respectively. The Na2-$O2B^a$ and Na2-$O1B^a$ distances are of 2.500(1) Å and 2.793(1) Å. The Na2-O1W bond length is equal to 2.374(1) Å. The sodium Na2 atom exhibits distorted an octahedral arrangement. The angles which would be 90° are in the range: 79.92(4)°-102.57(4)°, while those that would be 180° range from 124.17(4)° to 157.06(4)°. The bond distances and bond angles in the coordination polyhedra of sodium atoms are given in Table A1.

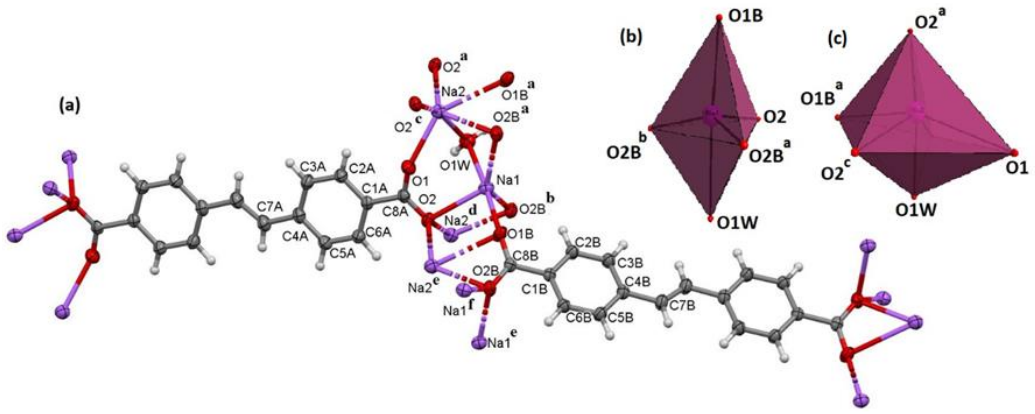

Fig 3. (a) Part of the crystal structure $\{[Na_2SDC(H_2O)]\}_n$ in ellipsoidal view of 50% probability level with numbering of atoms; coordination polyhedra of (b) Na1 and (c) Na2 atoms. Symmetry codes: (a) x, y-1,z; (b) x, -y+1.5,z-0.5; (c) x, -y+0.5, z+0.5, (d) x, -y+0.5, z-0.5; (e) x, y+1, z; (f) x, -y+1.5, z+0.5

In the crystal structure of the investigated sodium coordination polymer, two coordination modes of SDC^{2-} ligand can be distinguished (Fig. 4a and 4b). A-SDC and B-SDC forms of 4,4'-stilbenedicarboxylate ligand act as μ_8-bridging building blocks coordinating eight sodium centers. The ligand A-SDC behaves as an octadentate linker and coordinates sodium atoms through tetradentate-bridging carboxylate groups of (μ_4-η_1:η_3) character. The B-SDC ligand services as decadentate linker and coordinates metallic centers through pentadentate bridging-chelating carboxylate groups (μ_4-η_2:η_3). In both (A-SDC and B-SDC) ligands, the carboxylate groups are slightly rotated from the plane of the stilbenedicarboxylate ring. In the case of A-SDC molecule, the angle between the plane of the ring and the plane of the carboxylate group is 9.59°, whereas for the B-SDC molecule this angle is 15.74°. For the A-SDC linker, the angle of bridging carboxylate group is 123.4(1)°, while the lengths of the C8A-O2 and C8A-O1 bonds are 1.264(2) and 1.254(2) Å, respectively. In the B-SDC ligand, the angle of carboxylate group is 123.9(1)° and the C8B-O2B and C8B-O1B bond lengths are 1.260(2) and 1.253(2) Å, respectively. This sodium 4,4'-stilbenedicarboxylate complex has the form of three-dimensional coordination polymer as can be seen from the crystal packing diagram viewed along the *b* axis (Fig. 4c). The sodium atoms connected *via* carboxylate oxygen atoms and aqua ligand form characteristic two-dimensional inorganic-organic motifs extended in the *bc* plane which are further interconnected alternating organic layers composed of the same type of linker (A-SDC or B-SDC). These inorganic-organic motifs consist of regularly located Na1 and Na2 atoms (Fig. 4d).

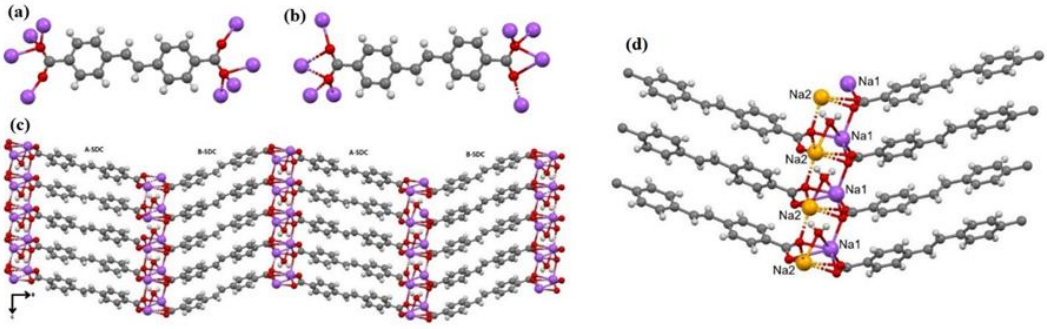

Fig 4. The two coordination modes of SDC ligand – (a) A-SDC and (b) B-SDC; (c) the representation of the three-dimensional coordination polymer $\{[Na_2SDC(H_2O)]\}_n$ in view along the *b* axis; (d) the part of inorganic-organic motif of sodium atoms in as-synthesized $\{[Na_2SDC(H_2O)]\}_n$ structure in view along the *b* axis

3.3. Reversibility of crystal-to-crystal transformation

3.3.1. ATR-FTIR investigations

The comparison of the infrared spectra of free ligand (H_2SDC) and its sodium coordination polymer allows to confirm complete deprotonation of both carboxylic group in metal complex that is evidenced

by the disappearance of characteristic bands from COOH groups such as: stretching vibrations of ν(C=O) at 1670 cm^{-1} and ν(C-O-H) at 1290 cm^{-1} within deformation vibrations of δ(OH) at 946 cm^{-1} (Fig. 5a and 5b). The infrared spectrum of $\{[Na_2SDC(H_2O)]\}_n$ exhibits weak broad band in the wavenumber range of 3500-3000 cm^{-1} and medium band at 1683 cm^{-1} assigned to the stretching ν(OH) and deformation vibrations δ(OH) of hydroxyl groups from coordinated water molecule. The ATR-FTIR spectrum of dehydrated form of sodium complex $[Na_2SDC]$ does not show these bands that confirm efficient removal of water from the complex structure (Fig 5c). The infrared spectra of sodium complexes show very diagnostic strong bands from asymmetric stretching vibrations of carboxylate groups $\nu_{asym}(COO)$ at 1536 cm^{-1} and 1532 cm^{-1}, respectively. Symmetric stretching vibrations of carboxylate groups $\nu_{sym}(COO)$ in the infrared spectra of sodium complexes appear at 1391 cm^{-1} and 1383 cm^{-1}, respectively. The slightly differences in the position of the asymmetric and symmetric stretching vibrations of the carboxylate groups in the discussed compounds may suggest different modes of sodium atoms coordination by these groups. This finding can be explained in the term of dehydration process which took place during isothermal heating of $\{[Na_2SDC(H_2O)]\}_n$ at 150°C. Elimination of water molecule from the coordination sphere of sodium atoms resulted in formation of vacant sites and implies an internal reorganization of the structure (Fernandez-Bartolome et al., 2022). As the result of such transformation, these sites may be occupied by other available electron pair donors. In the regarded anhydrous structure of sodium complex, additional coordination bonds between metal centers and carboxylate oxygen atoms can be formed due to great affinities of Na atoms to O-donor groups. This may change coordination fashion of carboxylate groups that is reflected in the frequencies of stretching vibrations of COO groups.

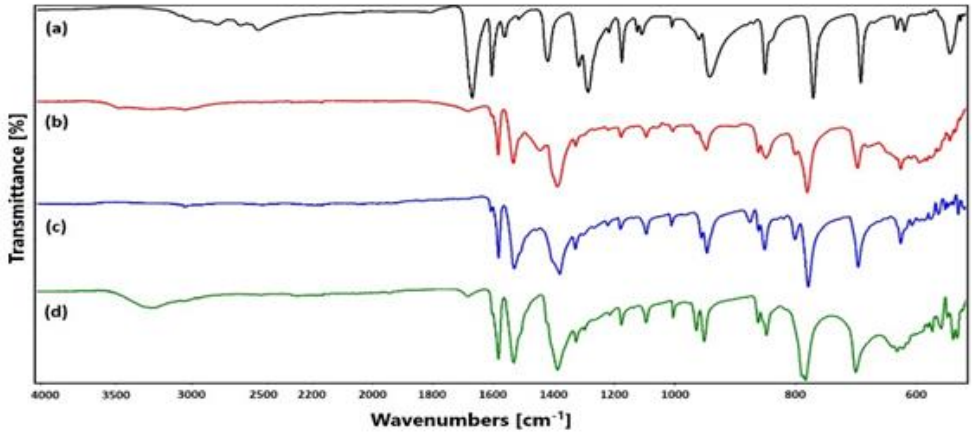

Fig. 5. Infrared spectra of (a) H_2SDC, (b) as-synthesized $\{[Na_2SDC(H_2O)]\}_n$, (c) anhydrous $[Na_2SDC]$ (heated at 150°C) and (d) rehydrated $[Na_2SDC(H_2O)]$

The infrared spectrum of sodium complex formed after immersion of dehydrated complex $[Na_2SDC]$ in water for several days is very similar to that of $\{[Na_2SDC(H_2O)]\}_n$. The diagnostic asymmetric and symmetric stretching vibrations of carboxylate groups appear at 1533 and 1390 cm^{-1}, respectively. The presence of broad band range from 3500 to 3000 cm^{-1} as well as medium strong band at 1683 cm^{-1} due to stretching and deformation vibrations of water molecules proves the re-incorporation of water molecules into the structure of the sodium complex (Fig. 5d).

The remaining sharp bands observed in the infrared spectra of all discussed compounds are connected with vibrations of 4,4'-stilbenedicarboxylate moieties. At wavenumber of 1585 cm^{-1} there is a sharp band from in-plane stretching vibrations $\nu(C_{Ar}C_{Ar})$. Characteristic bands for the aromatic system - deformation bands $\beta(C_{Ar}H)$ are present at 1330, 1225, 1182 and 1012 cm^{-1} (Pecile et al., 1969; Silverstein et al., 1998).

3.3.2. TG-DSC in air atmosphere

The thermal behaviour of all forms of sodium complexes was explored in air atmosphere by thermogravimetric (TG) method and differential scanning calorimetry (DSC). The recorded TG and DSC curves are given in Fig. 6.

The thermal decomposition of as-synthesized sodium complex $\{[Na_2SDC(H_2O)]\}_n$ occurs in two well-separated stages in air atmosphere. The first mass loss of 5.65% (calc. 5.45%) which takes place in the temperature range of 86-144°C is consistent with the water molecule departure from the structure of the coordination polymer. The liberation of aqua ligand is accompanied by an endothermic effect of ΔH=136 J/g with the peak top at 102°C (onset point 93°C) (Fig. 6b). The anhydrous form of sodium complex is thermally stable up to 491°C (Fig. 6a). Similar high thermal stability was observed for three-dimensional coordination polymer of sodium ions with 1,2,4-benzenetricarboxylic acid (Łyszczek et al., 2008). Such resistance on temperature stress may be explained in terms of the presence in their crystal structures inorganic-organic layers composed of tightly bonded Na atoms by carboxylate oxygen atoms. Further heating yields in mass loss of 43% due to its decomposition and combustion of organic part of the compound. This stage is dominated by the strong exothermic effect in the range 530-660°C with some submaxima at 570, 620 and 645°C. Such profile of DSC curve is characteristic of multi-stages burning process. The total mass loss of 55.54% at 700°C indicates an incomplete decomposition of investigated complex into the sodium carbonate.

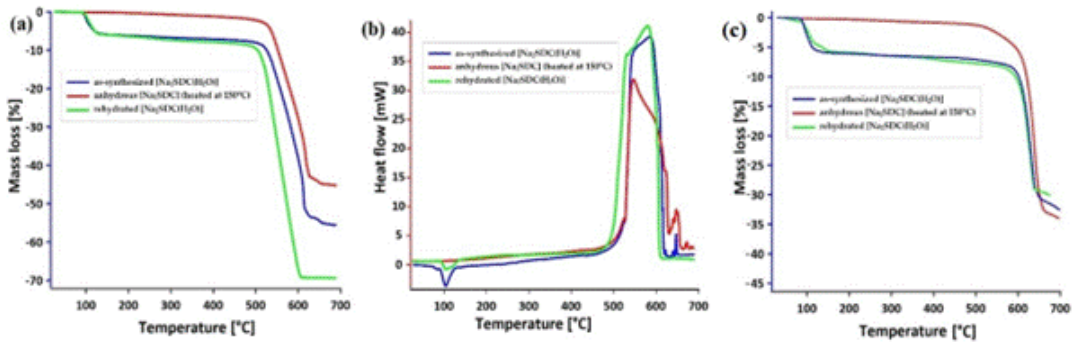

Fig. 6. The (a) TG and (b) DSC curves of: as-synthesized $\{[Na_2SDC(H_2O)]\}_n$ anhydrous $[Na_2SDC]$ (heated at 150°C) and rehydrated $[Na_2SDC(H_2O)]$ in air atmosphere according to legends; (c) the TG curves of as-synthesized $[Na_2SDC(H_2O)]$, anhydrous $[Na_2SDC]$ (heated at 150°C) and rehydrated $[Na_2SDC(H_2O)]$ in nitrogen atmosphere.

The TG curve of sodium complex obtained during evacuation of water molecules at 150°C shows no mass loss as well as energetic effects on the DSC curves up to 500°C (Fig. 6b). This observation confirms the effective removal of water molecules from the structure of metal complex. Next, the thermal decomposition and burning of organic ligand accompanied by strong exothermic effects took place. The observed solid residue of 54.84% found at 700°C implies not complete transformation into the stable sodium inorganic compound (Łyszczek et al., 2018).

The immersion of anhydrous form of complex in water gives the compound which is thermally stable up to 92°C. Mass loss of 5.95% in the temperature range of 93-147°C corresponds to the dehydration process. The endothermic effect of 145 J/g recorded at 105°C (onset point 94°C) associated with removal of water molecules is similar to that observed for pristine $\{[Na_2SDC(H_2O)]\}_n$. Dehydrated form of the complex is also highly thermally stable up to 495°C. The second significant mass loss of 60.80% observed in the temperature range 521-611°C was connected as it was mentioned previously with decomposition and burning processes. This stage was accompanied by very strong exothermic effect, with peak top at a temperature of 580°C. The total mass loss of 66.75% as well as pathways of the TG and DSC curves point out to complete decomposition of sodium complex, most likely into the Na_2CO_3 (Fig. 6) as can be deduced from the XRD pattern of solid residue which perfectly fits with the reference data of sodium carbonate 04-008-9670 (Gates-Rector et al., 2019).

A detailed analysis of the thermal data of the starting sodium complex as well as that obtained as a result of rehydration indicates that both compounds have identical composition. This fact leads us to assign the formula to the recrystallized form of sodium complex as $[Na_2SDC(H_2O)]$.

3.3.3. TG-FTIR in nitrogen atmosphere

The thermal behaviour of the investigated sodium complexes was also investigated in nitrogen atmosphere by coupled TG-FTIR method. Along with mass changes, the FTIR spectra of evolved gases

from investigated compounds decomposition were recorded. For the pristine complex $\{[Na_2SDC(H_2O)]\}_n$ the first mass loss of 5.91% (6.30% rehydrated form) visible in the range of 72-128°C (91-131°C) on the TG curve (Fig. 6c) is related to the dehydration of metal complexes as it can be seen from FTIR spectra. The infrared spectra recorded in that temperature range show characteristic bands in the wavenumber ranges 4000-3400 cm^{-1} and 2000-1200 cm^{-1} assigned to the stretching and deformation vibrations of evolved water molecules. At the same time, FTIR spectra of $[Na_2SDC]$ recorded from room temperature up to about 494°C do not show any bands as the result of compound thermal stability (Fig. 6c). The anhydrous forms of pristine and rehydrated complexes display thermal stability up to a temperature of 490 and 587°C, respectively. Further heating of all anhydrous sodium complexes in inert atmosphere up to 700°C yield in the decomposition process accompanied by mass losses of 30.49; 34.03 and 25.61% for compounds all investigated compounds (Fig. 6c). The total observed mass losses recorded during thermal decomposition of all studied sodium compounds are significantly lower in comparison to measurements in air due to incompleteness of organic moieties burning. The solid residues are a mixture of sodium carbonate, carbon, and some unidentified compounds.

The degradation of anhydrous sodium complexes is not only confirmed by the TG curves but also the FTIR spectra of the evolved gases. The stacked plot of the FTIR spectra of the liberated gases during the pristine complex decomposition is given in Fig. 7a. The infrared spectra of gaseous compounds exhibit diagnostic multi-top band in the wavenumber range 2400-2250 cm^{-1} and those in the range 750-600 cm^{-1} due to stretching and deformation vibrations of carbon dioxide. Along with carbon dioxide also molecules of carbon monoxide are liberated due to diagnostic double band with maxima 2185 and 2111 cm^{-1} (Głuchowska et al., 2022; Łyszczek et al., 2022). The presence of carbon oxides can be related to the breakage of sodium-oxygen as well as C_{Ar}-C_{carb} bonds between COO groups and stilbene moieties. Further heating of solid residue yielded in evolution besides carbon dioxide and water molecules also hydrocarbons – most probably methylbenzene, benzene and ethene molecules. The highest release of these gas products was observed after 30 minutes of sample heating (above 600°C) (Fig. 7a). It should be emphasized that formation of such gaseous is the effect of stilbene molecules cracking. In the wavenumber ranges 3150-3000 cm^{-1} and 3000-2800 cm^{-1} appear stretching vibrations of νCH groups from aromatic ring and methyl/methylene groups, respectively. Absorption bands at 1601, 1507 and 1496 cm^{-1} originate from vibrations of $\nu C_{Ar}C_{Ar}$ in the benzene ring of methylbenzene. The bands at 1457 and 1300 cm^{-1} derived from bending vibrations of methyl groups. The in-plane and out-of-plane bending CH vibrations were found at 1030 and 727 cm^{-1}, respectively. The reference spectrum of methylbenzene (toluene) along with the experimental spectrum recorded at 661 °C is given in Fig. A1b. The bands at 1040 and 669 cm^{-1} may be indicative for CH bending vibration of liberated benzene molecules. The weak bands at 957 and 826 cm^{-1} assigned to the wagging and rocking modes of CH_2 group also suggest liberation of an ethene molecules (Knaanie et al., 2016).

We have also investigated thermal decomposition of free 4,4′-stilbenedicarboxylic acid in nitrogen atmosphere. As can be seen in Fig. A1a, this dicarboxylic acid is thermally stable in inert atmosphere up to 338°C. In the temperature range of 339-474°C mass loss of 74.04% was observed due to its

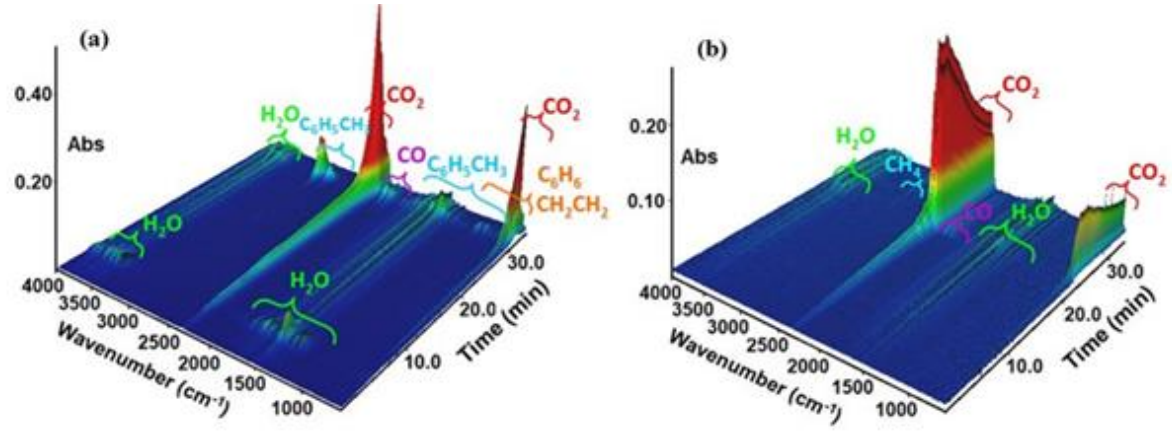

Fig. 7. Stacked plots of FTIR spectra of evolved gases during decomposition of (a) $\{[Na_2SDC(H_2O)]\}_n$ and (b) H_2SDC in nitrogen

decomposition.

The analysis of the FTIR spectra of evolved gases (Fig. 7b) allows to conclude that carbon oxides and water molecules are main volatile products of its decomposition. In contrast to the decomposition of sodium complexes described above, methylbenzene was not noticed as the gaseous product of free acid decomposition. At higher temperature, very weak band range from 3150 to 2800 cm^{-1} with maximum at 3014 cm^{-1} was assigned to the stretching vibrations of methane molecules. The total mass loss for H_2SDC decomposition was 79.50% at 700°C.

3.3.4. PXRD investigations

The XRD patterns of free H_2SDC acid, as-synthesized, dehydrated and rehydrated forms of the sodium complex (Fig. 8) were recorded due determination of structural changes caused by aqua ligand removal. The XRD pattern of free H_2SDC acid confirms phase purity of as-synthesized sodium complex. As can be seen from Fig. 8, anhydrous form of sodium complex retains crystallinity. The release of coordinated water molecule from the structure of the pristine sodium complex induces the *crystal-to-crystal* transformation. The XRD pattern of anhydrous form of complex approves formation of new crystal phase as can be pointed out from positions of diffraction peaks. Moreover, the storage of dehydrated complex in the water results in the formation of Na-O_{water} covalent bonds and the recovery of the original crystal structure (Fig. 8b and 8d). This fact points to the reversibility of hydration process in this novel three-dimensional sodium coordination polymer.

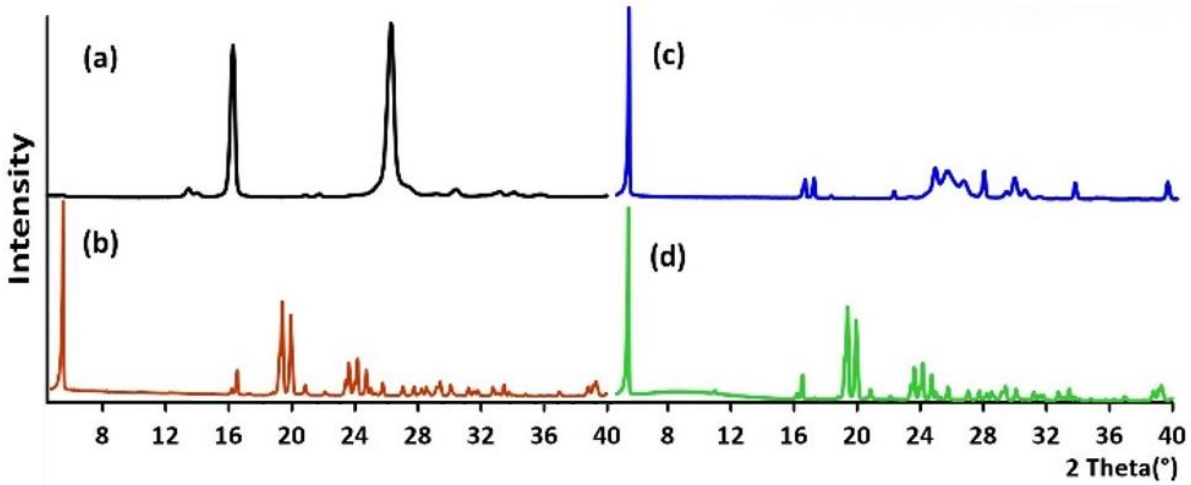

Fig. 8. PXRD patterns of (a) H_2SDC, (b) as-synthesized [$Na_2SDC(H_2O)$], (c) anhydrous [Na_2SDC] (heated at 150°C) and (d) rehydrated [$Na_2SDC(H_2O)$]

4. Conclusions

We have synthesized and characterized the first example of coordination polymer constructed by 4,4'-stilbenedicarboxylate ligand as linker and sodium ions as nodes. It worth to note that the compound was obtained from aqueous solution using Easymax 102 workstation with controlling *in-situ* reagents. The crystal structure of {[$Na_2SDC(H_2O)$]}n consists of inorganic-organic layers joined by 4,4'-stilbenedicarboxylate linkers of different coordination modes. Penta- and hexacoordinated sodium atoms are bonded by tetradentate-bridging and pentadentate bridging-chelating carboxylate groups into the three-dimensional framework. In the inner coordination sphere of metal centers appear also aqua ligands of bidentate-bridging character. Thermal decomposition of the studied complex takes place in two main stages connected with dehydration process and degradation of anhydrous framework as a result of node-linker breakage accompanied by linker combustion in air atmosphere. Decomposition of complex in nitrogen leads to the evolution of water, carbon oxides, methylbenzene, benzene and ethene molecules whereas free acid degrades with liberation of small molecules. We also reveal reversibility of *crystal-to-crystal* transformation which took place during hydration-rehydration processes.

Appendix A

Table A1. The bond distance and bond angles between the atoms present in the structure of as-synthesized [$Na_2SDC(H_2O)$]

Na1		Na2	
Bond distance (Å)			
Na1-O2	2.483(1)	Na2-O2[a]	2.428(1)
Na1-O1W	2.368(1)	Na2-O1W	2.374(1)
Na1-O2B[a]	2.449(1)	Na2-O2[c]	2.487(1)
Na1-O2B[b]	2.320(1)	Na2-O1	2.346(1)
Na1-O1B	2.298(1)	Na2-O2B[a]	2.500(1)
		Na2-O1B[a]	2.793(1)
Bond Angles (°)			
O2B[b]-Na1-O1W	81.72(4)	O1W-Na2-O1B	80.15(4)
O2-Na1-O1W	89.77(4)	O1W-Na2-O1	79.92(4)
O2B[a]-Na1-O1W	77.82(4)	O1-Na2-O2[c]	85.10(4)
O2B[b]-Na1-O1B	100.51(4)	O2[c]-Na2-O1B[a]	102.57(3)
O2-Na1-O1B	86.76(4)	O2B[a]-Na2-O2A[a]	124.17(4)
O2B[a]-Na1-O1B	102.68(4)	O1W-Na2-O2[a]	157.04(4)
O2-Na1-O2B[a]	127.83(4)	O2[a]-Na2-O2[c]	123.96(3)
O2B[a]-Na1-O2B[b]	134.34(4)	O1W-Na2-O2B[a]	76.69(4)
O2B[b]-Na1-O2	92.08(4)	O2[a]-Na2-O2B[a]	87.83(3)
		O2[a]-Na2-O1B[a]	77.67(3)
		O2B-Na2-O1B[a]	49.16(3)
Symmetry codes: (a) x, y-1, z; (b) x,-y+1.5, z-1/2; (c) x, -y+1/2, z+1/2			

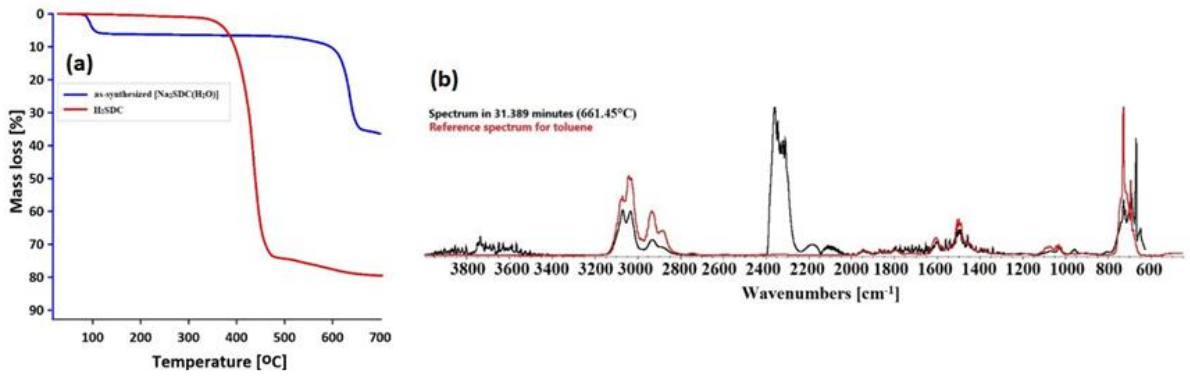

Fig. A1. (a) The TG curves of as-synthesized [$Na_2SDC(H_2O)$] and H_2SDC in nitrogen atmosphere; (b) the spectrum of gaseous decomposition products in 31.389 minutes with the reference spectrum of toluene

References

ALLEN, F.H., 2002. *The Cambridge Structural Database: a quarter of a million crystal structures and rising*. Acta Crystallogr B. *58*, 380-388.

ALOTHMAN, Z.A., 2012. *A Review: Fundamental Aspects of Silicate Mesoporous Materials*. Materials. 5, 2874-2902.

BAUER, C.A., TIMOFEEVA, T.V., SETTERSTEN, T.B., PATTERSON, B.D., LIU, V.H., SIMMONS, B.A., ALLENDORF, M.D., 2007. *Influence of Connectivity and Porosity on Ligand-Based Luminescence in Zinc Metal−Organic Frameworks*. Journal of the American Chemical Society. 129, 7136-7144.

BIRADHA, K., RAMANAN, A., VITTAL, J., 2009. *Coordination Polymers Versus Metal−Organic Frameworks.* Crystal Growth & Design. 9, doi:10.1021/cg801381p.

BOXI, S., JANA, D., GHORAI, B.K., 2019. *Synthesis and optical properties of bipolar quinoxaline-triphenylamine based stilbene compounds*. Optical Materials. 1, 100013.

CAO, J., LI, X., TIAN, H., 2020. *Metal-Organic Framework (MOF)-Based Drug Delivery.* Current Medicinal Chemistry. 27, 5949-5969.

CHEN, J., XIN, Y., WU, J., LIAO, P., CHEN, L., ZHANG, J., 2021. *Supported Metal Nanoparticles in Metal-Organic Monoliths for Assembly of a Catalytic Microfluidic Reactor.* ChemNanoMat. 7, 334-340.

CrysAlisPRO Software System, Rigaku: Oxford, UK,. 2016.

DENG, Z.-P., HUO, L.-H., WANG, H.-Y., GAO, S., ZHAO, H., 2010. *A series of three-dimensional lanthanide metal organic frameworks with biphenylethene-4,4'-dicarboxylic acid: Hydrothermal syntheses and structures.* CrystEngComm. 12, 1526-1535.

DIMAS CHANDRA PERMANA, A., OMAR, A., GUILLERMO GONZALEZ-MARTINEZ, I., OSWALD, S., GIEBELER, L., NIELSCH, K., MIKHAILOVA, D., 2022. *MOF-Derived Onion-Like Carbon with Superior Surface Area and Porosity for High Performance Lithium-Ion Capacitors.* Batteries & Supercaps. *5*, e202100353.

FAN, W., ZHANG, X., KANG, Z., LIU, X., SUN, D., 2021. *Isoreticular chemistry within metal–organic frameworks for gas storage and separation.* Coordination Chemistry Reviews**.** *443*, 213968.

FAN, L., YU, Q., CHEN, J., KHAN, U., WANG, X., GAO, J., 2022. *Achievements and Perspectives in Metal&ndash, Organic Framework-Based Materials for Photocatalytic Nitrogen Reduction*. Catalysts. 12, 1005.

FARRUGIA, L., 1999. *WinGX suite for small-molecule single-crystal crystallography*. Journal of Applied Crystallography. 32, 837-838.

FERNANDEZ-BARTOLOME, E., MARTINEZ-MARTINEZ, A., RESINES-URIEN, E., PIÑEIRO-LOPEZ, L., COSTA, J.S., 2022. *Reversible single-crystal-to-single-crystal transformations in coordination compounds induced by external stimuli.* Coordination Chemistry Reviews. 452, 214281..

FU, H.-R., WANG, N., WU, X.-X., LI, F.-F., ZHAO, Y., MA, L.-F., DU, M., 2022. *Circularly Polarized Room-Temperature Phosphorescence and Encapsulation Engineering for MOF-Based Fluorescent/Phosphorescent White Light-Emitting Devices*. Advanced Optical Materials, 8, 2000330.

GATES-RECTOR, S., BLANTON, T., 2019. *The Powder Diffraction File: A Quality Materials Characterization Database*. Powder Diffraction. 34(4), 352-360.

GŁUCHOWSKA, H., ŁYSZCZEK, R., JUSZA, A., PIRAMIDOWICZ, R., 2022. *Effect of N,N'-dimethylformamide solvent on structure and thermal properties of lanthanide(III) complexes with flexible biphenyl-4,4'-dioxydiacetic acid.* Journal of Thermal Analysis and Calorimetry. 147, 1187-1200.

GŁUCHOWSKA, H., ŁYSZCZEK, R., MAZUR, L., KIRILLOV, A.M., 2021. *Structural and Thermal Investigations of Co(II) and Ni(II) Coordination Polymers Based on biphenyl-4,4'-dioxydiacetate Linker*. Materials. 14, 3545.

HOU, J., CHEN, X., SUN, J., FANG, Q., 2020. *A facile conversion of a bio-based resveratrol to the high-performance polymer with high Tg and high char yield*. Polymer. 200, 122570.

HU, H., WANG, Z., CAO, L., ZENG, L., ZHANG, C., LIN, W., WANG, C., 2021. *Metal-organic frameworks embedded in a liposome facilitate overall photocatalytic water splitting*. Nat Chem. 13, 358-366.

HUANG, Y., ZHANG, J., YUE, D., CUI, Y., YANG, Y., LI, B., QIAN, G. *Solvent-Triggered Reversible Phase Changes in Two Manganese-Based Metal–Organic Frameworks and Associated Sensing Events*. Chemistry – A European Journal. 24, 13231-13237.

KNAANIE, R., ŠEBEK, J., TSUGE, M., MYLLYS, N., KHRIACHTCHEV, L., RÄSÄNEN, M., ALBEE, B., POTMA, E.O., GERBER, R.B., 2016. *Infrared Spectrum of Toluene: Comparison of Anharmonic Isolated-Molecule Calculation and Experiments in Liquid Phase and in a Ne Matrix*. J Phys Chem A., 120, 3380-3389.

KUZNETSOVA, A., MATVEEVSKAYA, V., PAVLOV, D., YAKUNENKOV, A., POTAPOV, A., 2020. *Coordination Polymers Based on Highly Emissive Ligands: Synthesis and Functional Properties*. Materials. 13, 2699.

LEE, Y.H., KWON, Y., KIM, C., HWANG, Y.E., CHOI, M., PARK, Y., JAMAL, A., KOH, D.Y., 2021. *Controlled Synthesis of Metal-Organic Frameworks in Scalable Open-Porous Contactor for Maximizing Carbon Capture Efficiency*. JACS Au. 1, 1198-1207. LEE, J.H., JAWORSKI, J., JUNG, J.H., 2013. *Luminescent metal–organic framework-functionalized graphene oxide nanocomposites and the reversible detection of high explosives*. Nanoscale. 5, 8533-8540.

LI, X., BIAN, H., HUANG, W., YAN, B., WANG, X., ZHU, B., 2022. *A review on anion-pillared metal–organic frameworks (APMOFs) and their composites with the balance of adsorption capacity and separation selectivity for efficient gas separation*. Coordination Chemistry Reviews. 470, 214714.

LI, Y., SONG, D., 2011. *Syntheses, structures and luminescent properties of decorated lanthanide metal-organic frameworks of (E)-4,4'-(ethene-1,2-diyl)dibenzoic acids*. CrystEngComm. 13, 1821-1830.

LIU, W.-L., LO, S.-H., SINGCO, B., YANG, C.-C., HUANG, H.-Y., LIN, C.-H., 2013. *Novel trypsin–FITC@MOF bioreactor efficiently catalyzes protein digestion*. Journal of Materials Chemistry B. 1, 928-932.

LUO, H.-B., REN, Q., WANG, P., ZHANG, J., WANG, L., REN, X.-M., 2019. *High Proton Conductivity Achieved by Encapsulation of Imidazole Molecules into Proton-Conducting MOF-808*. ACS Applied Materials & Interfaces. 11, 9164-9171.

ŁYSZCZEK, R., RUSINEK, I., OSTASZ, A., SIENKIEWICZ-GROMIUK, J., VLASYUK, D., GROSZEK, M., LIPKE, A., PAVLYUK, O., 2021. *New coordination polymers of selected lanthanides with 1,2-phenylenediacetate linker: Structures, thermal and luminescence properties*. Materials. 14, doi:10.3390/ma14174871.

ŁYSZCZEK, R., RUSINEK, I., SIENKIEWICZ-GROMIUK, J., IWAN, M., PAVLYUK, O., 2019. *3-D lanthanide coordination polymers with the flexible 1,3-phenylenediacetate linker: Spectroscopic, structural and thermal investigations*. Polyhedron. 159, 93-101.

ŁYSZCZEK, R., VLASYUK, D., PODKOŚCIELNA, B., GŁUCHOWSKA, H., PIRAMIDOWICZ, R., JUSZA, A., 2022. *A Top-Down Approach and Thermal Characterization of Luminescent Hybrid BPA.DA-MMA@Ln2L3 Materials Based on Lanthanide(III) 1H-Pyrazole-3,5-Dicarboxylates*. Materials. 15, doi:10.3390/ma15248826.

ŁYSZCZEK, R., MAZUR, L., RZĄCZYŃSKA, Z., 2008. *A three-dimensional coordination polymer constructed from sodium(I) ion and benzene-1,2,4-tricarboxylate ligand: Thermal, structure and spectroscopic characteristics*. Inorganic Chemistry Communications. 11, 1091-1093.

ŁYSZCZEK, R., GŁUCHOWSKA, H., MAZUR, L., TARASIUK, B., KINZHYBALO, V., KIRILLOV, A.M. 2018 *Structural diversity of alkali metal coordination polymers driven by flexible biphenyl-4,4'-dioxydiacetic acid*. Journal o Solid State Chemistry, 265, 92-99.

MALLAKPOUR, S., NIKKHOO, E., HUSSAIN, C.M., 2022. *Application of MOF materials as drug delivery systems for cancer therapy and dermal treatment*. Coordination Chemistry Reviews. 451, 214262.

MOGALE, R., AKPOMIE, K.G., CONRADIE, J., LANGNER, E.H.G., 2022. *Isoreticular aluminium-based metal-organic frameworks with structurally similar organic linkers as highly efficient dye adsorbents*. Journal of Molecular Structure. 1268, 133648.

NING, E., YANG, L., TU, B., PANG, Q., LI, X., XU, H., QI, Y., LI, Q., 2019. *Interface construction in microporous metal organic frameworks from luminescent terbium-based building blocks*. Journal of Colloid and Interface Science. 552, 372-377.

OMWOMA, S., 2020. *Trace Metal Detection in Aqueous Reservoirs Using Stilbene Intercalated Layered Rare-Earth Hydroxide Tablets*. Journal of Analytical Methods in Chemistry. 2020, 9712872, doi:10.1155/2020/9712872.

PE III, J., MUN, J., MUN, S., 2023. *Thermal characterization of kraft lignin prepared from mixed hardwoods.* BioResources. 18, 926-936.

PECILE, C., LUNELLI, B., 1969. *Infrared spectra of trans-1,2-diphenylethylene and trans-1,2-diphenylethylene-d12*. Canadian Journal of Chemistry. 47, 243-250. SHELDRICK, G., 2015. *Crystal structure refinement with SHELXL*. Acta Crystallographica Section C. 71, 3-8.

SILVERSTEIN R. M., F.X.W., KIEMLE D. J., 1998. *Spectrometric identification of organic compounds*, Wiley&Sons. pp. 546-553.

TEO, W.L., ZHOU, W., QIAN, C., ZHAO, Y., 2021. *Industrializing metal–organic frameworks: Scalable synthetic means and their transformation into functional materials*. Materials Today. 47, 170-186.

VEK, V., POLJANŠEK, I., CERC KOROŠEC, R., HUMAR, M., OVEN, P., 2022. *Impact of steam-sterilization and oven drying on the thermal stability of phenolic extractives from pine and black locust wood*. Journal of Wood Chemistry and Technology. 42, 467-477.

WEI, W., XIA, Z., WEI, Q., XIE, G., CHEN, S., QIAO, C., ZHANG, G., ZHOU, C., 2013. *A heterometallic microporous MOF exhibiting high hydrogen uptake*. Microporous and Mesoporous Materials. 165, 20-26.

WU, S., XING, X., WANG, D., ZHANG, J., CHU, J., YU, C., WEI, Z., HU, M., ZHANG, X., LI, Z., 2020. *Highly Ordered Hierarchically Macroporous MIL-125 with High Specific Surface Area for Photocatalytic CO2 Fixation*. ACS Sustainable Chemistry & Engineering. 8, 148-153.

XUAN, W., ZHU, C., LIU, Y., CUI, Y., 2012. *Mesoporous metal–organic framework materials*. Chemical Society Reviews. 41, 1677-1695.

YAN, X., CHEN, L., SONG, H., GAO, Z., WEI, H., REN, W., WANG, W., 2021. *Metal–organic framework (MOF derived catalysts for chemoselective hydrogenation of nitroarenes.* New Journal of Chemistry. 45, 18268-18276.

YANG, X.-L., DING, C., GUAN, R.-F., ZHANG, W.-H., FENG, Y., XIE, M.-H., 2021. *Selective dual detection of H_2S and Cu^{2+} by a post-modified MOF sensor following a tandem process*. Journal of Hazardous Materials. 403, 123698.

YU, Y., BRIÓ PÉREZ, M., CAO, C., DE BEER, S., 2021. *Switching (bio-) adhesion and friction in liquid by stimulus responsive polymer coatings.* European Polymer Journal. 147, 110298.

ZHANG, J., YAO, S., LIU, S., LIU, B., SUN, X., ZHENG, B., LI, G., LI, Y., HUO, Q., LIU, Y., 2017. *Enhancement of Gas Sorption and Separation Performance via Ligand Functionalization within Highly Stable Zirconium-Based Metal Organic Frameworks*. Crystal Growth & Design. 17, 2131-2139.